International Journal of Minerals, Metallurgy and Materials
Volume 27, Number 6, June 2020, Page 801
https://doi.org/10.1007/s12613-020-2017-0

Effect of the initial ECAP passes on crystal texture and residual stresses of 5083 aluminum alloy

L. Romero-Reséndiz[1),*], *A. Flores-Rivera*[1),*], *I.A. Figueroa*[1)], *C. Braham*[2)], *C. Reyes-Ruiz*[3)], *I. Alfonso*[4)], *and G. González*[1)]

1) Instituto de Investigaciones en Materiales, Universidad Nacional Autónoma de México, Cd. de México 04510, México
2) Procédés et Ingénierie en Mécanique et Matériaux, Arts et Métiers, Paris 75013, France
3) Departamento de Diseño y Manufactura, Facultad de Ingeniería, Universidad Nacional Autónoma de México, PIIT Apodaca 66629, México
4) Instituto de Investigaciones en Materiales, Unidad Morelia, Universidad Nacional Autónoma de México, Morelia 58190, México
(Received: 23 November 2019; revised: 10 February 2020; accepted: 12 February 2020)

Abstract: To produce a highly refined microstructure, several metals or alloys have been processed via equal-channel angular pressing (ECAP). In this work, the mechanical and microstructural changes of the 5083 aluminum alloy in H11 condition after processed by two ECAP passes were investigated. An ECAP H13 steel die with an inner angle (α) of 120° and outer curvature (β) of 20° was used. The microstructural changes were associated with the loss of texture symmetry. The morphologies of the Mg_2Si and α-Al(Mn,Fe)Si precipitates for the sample at the initial condition were similar to those subjected to two ECAP passes. The peak broadening measured by X-ray diffraction revealed an increment of both grain refinement and microstrain. After the second extrusion pass, the hardness increased by 62% compared with the initial condition. Moreover, the heterogeneous hardness behavior was compatible with a highly localized dislocation density. After two ECAP passes, shear parallel bands were observed to be at nearly 45° to the extrusion direction. The evaluation of first-order residual stress as a function of the depth of the analyzed sample displayed compressive or tensile values, depending on the measured face. With the plastic deformation applied, the first and second-order residual stresses exhibited significant increment. Williamson-Hall plots showed positive slopes, indicating an increment in the microstrain.

Keywords: aluminum alloy; equal-channel angular pressing; texture; microstructure; residual stress

1. Introduction

Equal-channel angular pressing (ECAP) is a successful process for generating nanostructures, aiming to improve the mechanical properties of components with potential industrial applications. Despite their wide technological applications in areas such as the marine, automotive, and aerospace industries [1], the 5083 aluminum alloy has rarely been studied under severe plastic conditions. Compared with other aluminum alloys, 5083 Al alloy has some advantages, which include good mechanical properties [2], high corrosion resistance, formability [3], and superplasticity behavior [4]. The 5083 Al alloy possesses a higher ultimate tensile strength compared with other aluminum alloys after equal-channel-angular-pressed (ECAPed); this is due to its high Mg content and microstructure with sub-micrometric and micrometric grains [5].

Studies on the ECAP of 5083 Al alloy are mainly focused on the change of the second-phase morphology, reporting the fragmentation of second phases as a function of the ECAP passes and the distribution of such fragmented particles throughout the sample [6]. Several researchers [7] have also studied the dependence of the 5083 alloy tensile behavior on the ECAP temperature. Lee *et al.* [8] reported a reduction in the recovery temperature, recrystallization, and precipitation with an increase in the number of passes. However, the existing studies on the ECAPed 5083 Al alloy did not investigate the presence of the residual stresses induced by the process. This is important, as such stresses have a strong effect on the mechanical properties. In addition, measuring the residual stresses helps in detecting stress concentration zones that can promote failure [9]. Moreover, the

*These authors contributed equally to this work.
Corresponding author: G. González E-mail: joseggr@unam.mx

texture evolution generated in the 5083 alloy by the ECAP process has rarely been reported in the literature. This is important as it is considered a relevant microstructural effect in forming processes.

Considering the above, the aim of this work is to study the evolution of the profile stress state and assess the effect of the friction between the die and the sample. Residual stress measurements were also carried out at different depths to evaluate the effect of the ECAP process. The texture and obtained microstructures for samples at the initial condition and after one and two ECAP passes were also examined.

2. Experimental

Commercial 5083 H11 aluminum alloy was used as the starting material, with a nominal composition (wt%) of 4.0−4.9 Mg, 0.4−1.0 Mn, 0.4 Si, 0.4 Fe, 0.25 Zn, 0.05−0.25 Cr, 0.18 Ti, 0.1 Cu, and Al balance. Bars of 16 mm × 16 mm × 120 mm were cut for the ECAP analysis. The ECAP H13 steel die set had an inner angle (α) of 120°, an outer curvature (β) of 20°, and a channel with a square section of 16 mm per side. The schematic representation of the experimental setup, the angles of the ECAP die, and the location where the specimens were taken for the different characterizations are displayed in Figs. 1(a), 1(b), and 1(c), respectively. In Fig. 1(c), ND, TD, and ED are the normal, transversal, and extrusion directions, respectively; TP, EP, and NP are the transversal, extrusion, and normal planes, respectively. The Bc route (rotation along its longitudinal axis by 90° clockwise) at room temperature was carried out between passes. This route was employed to obtain higher grain refinement compared with those of other routes [10] and generate greater homogeneity in the extruded products [11]. Moreover, MoS_2 lubricant was used to reduce the friction between the sample and the die walls. The alloy was extruded up to two passes with a pressing speed of 1 mm·s^{-1}. According to Iwahashi's equation [12] and the die geometry, every single ECAP pass generates a deformation of 0.63, which becomes accumulative for consecutive passes. From this point, the sample without deformation is named 0P, and the samples subjected to one and two ECAP passes are named 1P and 2P, respectively.

The microscopic analysis of the samples, taken from the extrusion plane (EP in Fig. 1(c)), was carried out on a JEOL 7600F scanning electron microscope (SEM). Before the microstructural examination, using alumina abrasive of 0.1 μm, the surfaces of the samples were prepared to obtain a mirror finish appearance. Lamellas for transmission electron microscopy (TEM) analysis (JEOL 120EX) were obtained by focus ion beam microscopy (JEOL-9320FIB). The X-ray diffraction (XRD) measurements were performed using a Philips X'pert diffractometer, with Cu K_α radiation and 30 kV and 35 mA as the voltage and current conditions, respectively. The texture analysis was performed in the normal plane (NP) of the processed samples (Fig. 1(c)), and pole figures for (111), (200), and (220) planes were taken. Rigaku-3D EXPLORE 2.5 software and MTEX (Matlab toolbox R2014b) were used to display data and calculate the orientation distribution functions (ODFs), respectively.

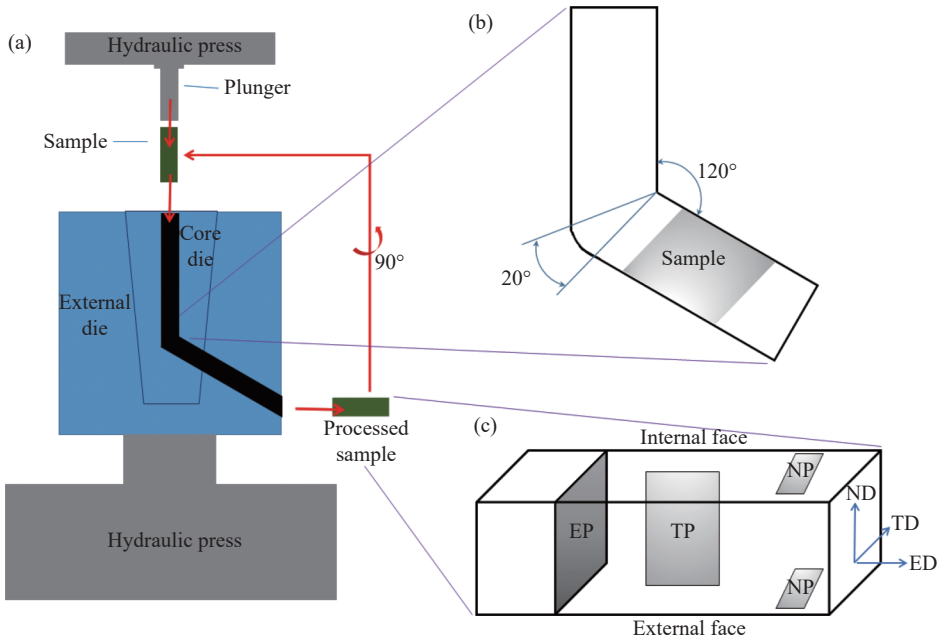

Fig. 1. (a) Schematic representation of the ECAP experimental setup used in this study; (b) angles in the extrusion channel; (c) planes where the samples were taken for the characterization. Here, ND, TD, and ED are the normal, transversal, and extrusion directions, respectively; TP, EP, and NP are the transversal, extrusion, and normal planes, respectively.

For residual stress study, a diffractometer Set-X was used. The samples for this analysis were electrochemically polished with 85vol% ethanol, 10vol% 2-butoxyethanol, and 5vol% water solution under 10 A and 5 V. Measurements from the superficial NP (Fig. 1(c)) to a depth of 80 μm were conducted by taking values every 20 μm. The macro-residual stresses (order I) were evaluated on the internal (top) and external (bottom) faces of the NP (Fig. 1) using the $\sin^2\psi$ method. Bruker-STRESS software was used for calculating the stress values. This technique assumes that the macro-strain is uniform over relatively large distances, namely several grains; the macro-strain is deduced from measuring the diffraction peak shift as a function of angles ψ and φ, where ψ is the angle subtended by the bisector of the incident and diffracted beam and the surface normal, and φ is the angle that describes the direction of the measurement.

The micro-residual stresses (orders II and III) were determined in the EP (Fig. 1(c)). Rietveld refinement calculated by FULLPROF 2017 version was used for obtaining the lattice parameters and the peak broadening. This technique focuses on the strain that occurred inside the grain, which is measured by the corresponding diffraction peak broadening. Finally, through the elastic tensor for a specific material, the strain can be converted to stress values. The instrumental broadening was evaluated with LaB_6 powder. The evolution of microstrains was assessed using Williamson-Hall plots. This analytical procedure can be found in detail in a previous work [13].

A Shimadzu microdurometer model HMV-2000 was used to determine the microhardness on the EP (Fig. 1(c)). For this purpose, a load of 1 N was employed for 10 s. A total of 70 measurements were taken per sample.

3. Results and discussion

Fig. 2 shows the presence of two phases: the dark gray zones correspond to Mg_2Si precipitates, which are second-phase particles found in Al 5xxx alloys [14−15]; the light gray zones are α-Al(Mn,Fe)Si phase. Similar results have been reported for other Al alloys [14].

The chemical composition of the α-Al(Mn,Fe)Si phase can be different depending on the initial chemical contents and the thermal history [15−16]. In the present case, the mean composition of the α-phase was 58wt% Al, 13wt% Mn, 24wt% Fe, and 5wt% Si. The chemical compositions of both phases are congruent with the preexisting particles reported in other works for the same 5083 alloy [17−18]. The morphologies of the Mg_2Si and α-Al(Mn,Fe)Si precipitates for the 0P and 2P samples were similar (Figs. 2(a) and 2(b)). Fig. 2(c) shows the zoomed XRD pattern of the diffraction peaks generated from the Mg_2Si and the α-Al(Mn,Fe)Si phases in the 2P sample.

As can be seen in Fig. 3(a), the initial microstructure showed fine precipitates homogeneously distributed in the sample. In contrast, as an effect of the two ECAP passes, shear parallel bands at nearly 45° to the extrusion direction

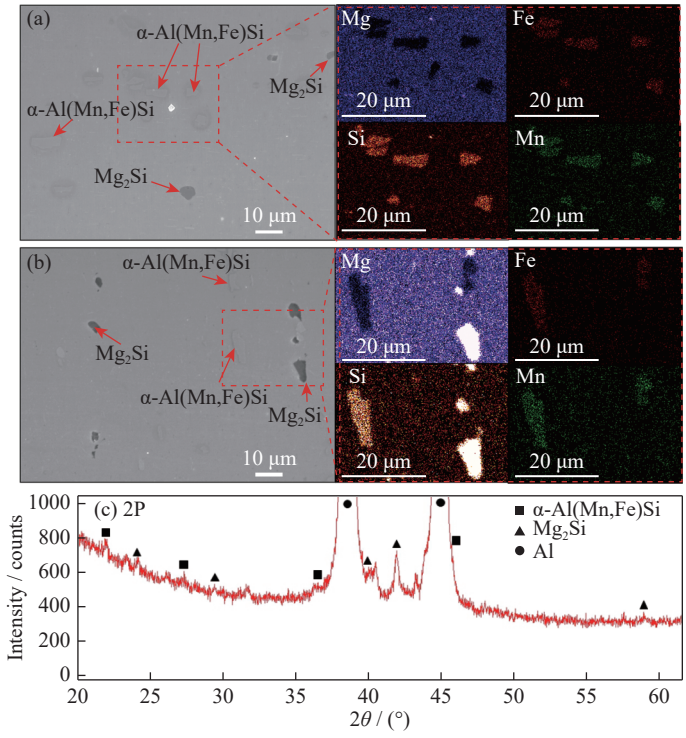

Fig. 2. SEM microstructures and energy-dispersive X-ray spectroscopy mapping in the extrusion plane (EP) for the (a) 0P and (b) 2P samples; (c) zoomed XRD pattern showing the secondary phases in the 2P sample.

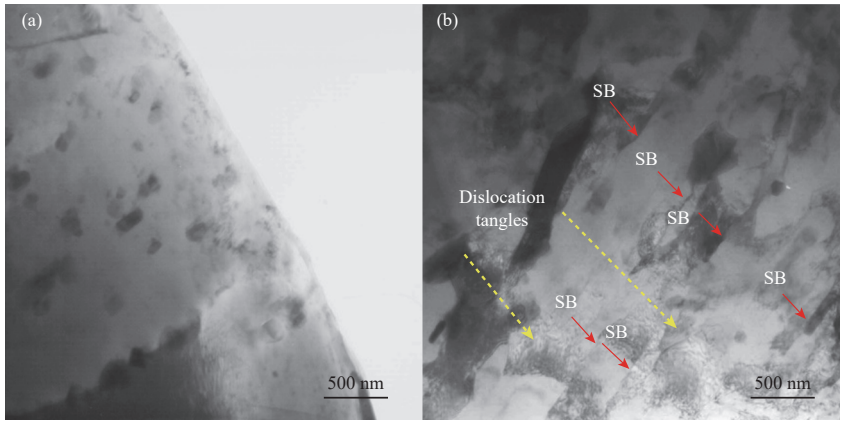

Fig. 3. TEM microstructures in the EP for the (a) 0P and (b) 2P samples, showing the presence of shear bands (SB) and dislocation tangles.

were observed (Fig. 3(b)). The microstructure analysis showed a successful grain refinement and the presence of subgrains inside the grain, which was expected after the initial ECAP passes [19−20]. Dislocations were also observed inside the grains, indicated by the dotted arrows in Fig. 3(b). The comparison between Figs. 3(a) and 3(b) allowed observing the increment of dislocation density after two ECAP passes, which was a result of the applied deformation.

Fig. 4 shows the presence of subgrains that were formed as a result of the deformation process after the second ECAP pass. These subgrains changed from white to black zones in the diffraction position when the sample was rotated from 0° to 4° with the double tilt holder. Dislocation tangles occurred after two extrusion passes, and the characteristic shapes of the Mg_2Si precipitates were also observed (Fig. 4).

To evaluate the effect of the microstructural reorganization over the macrotexture, ODFs were obtained (Fig. 5). These ODFs showed the presence of texture components ex-

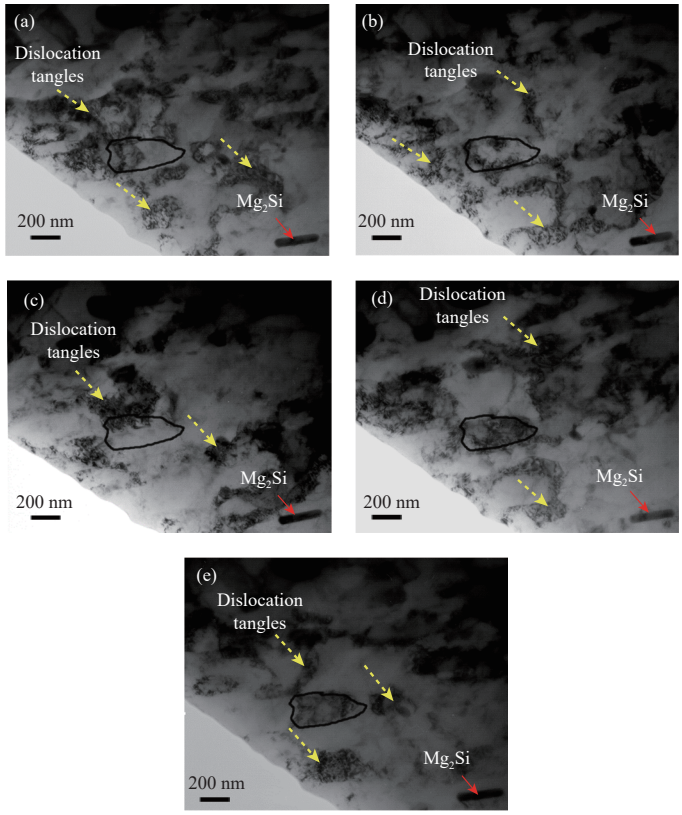

Fig. 4. TEM images showing subgrains after the second ECAP pass, observed from different rotation angles: (a) 0°; (b) 1°; (c) 2°; (d) 3°; (e) 4°. The original grain is indicated by the black loop; the yellow and red arrows indicate dislocation tangles and Mg_2Si precipitates, respectively.

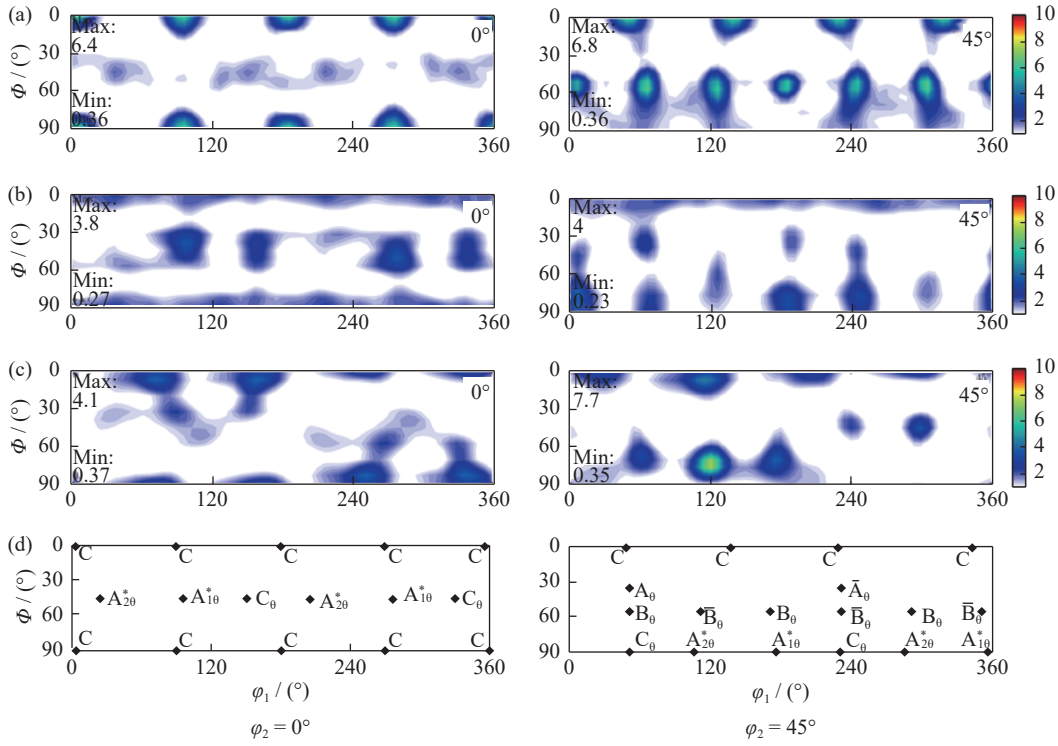

Fig. 5. φ_2 **sections of the orientation distribution functions for (a) 0P, (b) 1P, and (c) 2P samples; (d) key of ideal texture components of the ODFs.**

pected for a simple shear process on face-centered cubic (FCC) metals, with an extrusion angle of 120° [21]. The ODFs were calculated with triclinic sample symmetry.

After the ODFs analysis, the initial texture components $A^*_{2\theta}$, C_θ, B_θ, and $\overline{B}_\theta$ were identified. At the first ECAP pass, the component $A^*_{2\theta}$ lost intensity and the $A^*_{1\theta}$ component appeared. The remaining textures of B_θ and $\overline{B}_\theta$ were observed in the 1P and 2P samples. The cube texture indicated by "C" in Fig. 5(d) was observed for the 0P sample, but as the number of passes increased, the intensity of such texture dropped. The loss of intensity could be related to the formation of randomly organized new grains as a function of the ECAP passes, which was associated with the subgrains formation shown in Fig. 4. As observed in Fig. 5, the texture intensity symmetry changed from monoclinic (two-fold axis around the ND axis of the sample) to triclinic (one-fold axis of symmetry). This loss of symmetry indicated that the texture was rotated between passes around an axis, which was not the texture-symmetry-axis of the process, as expected for Bc and Ba routes [21].

To illustrate the effect of the microstructure on the mechanical behavior, the microhardness mappings for samples 0P and 2P were carried out. From Fig. 6, the hardness for the 2P sample almost doubled that obtained for the initial-condition 0P sample. When analyzing the mapping, it is evident that heterogeneous hardness values were obtained, indicating that the ECAP process induced a heterogeneous deformation state. The localized plastic deformation in ECAP was promoted by the heterogeneous deformation [22].

The average hardness values for the 0P and 2P samples were 784.6 and 1275 MPa, respectively. The increase in hardness after the first ECAP pass has been reported by other authors [23]. This heterogeneous hardness behavior was compatible with a highly localized dislocation density. The hardness values divided by a factor of 3 could be considered a good approximation of the yield strength (YS) [24–26]. If this relation was applied, the 0P and 2P samples obtained YS of 261.5 and 425 MPa, respectively.

Due to the nature of the ECAP process, one part of the energy applied is kept as elastic energy, producing residual stresses. Fig.7 shows the results for the residual stress profiles for the internal and external faces. Two zones were identified: zone I, from the surface to a depth of 20 μm; zone II, from 20 to 80 μm. Zone I is considered a mixture of the friction effect (die and sample) and ECAP process, and zone II is representative of the residual stress generated only by the ECAP process. In general terms, the 1P sample showed compressive values, or these values could be assumed as neutral, since the magnitude of the residual stress is less than 5% of the YS (Figs. 7(a) and 7(b)), while the 2P sample showed higher compressive values for the external face, with a positive slope for the deepest analyzed zone (Fig. 7(c)). For the 2P sample, the formation of a plateau from 20 to 60 μm was observed. This could indicate that the stress was rather constant, being consistent with the deformation of this zone. For the internal face (Fig. 7(d)), a tensile tendency with a positive slope

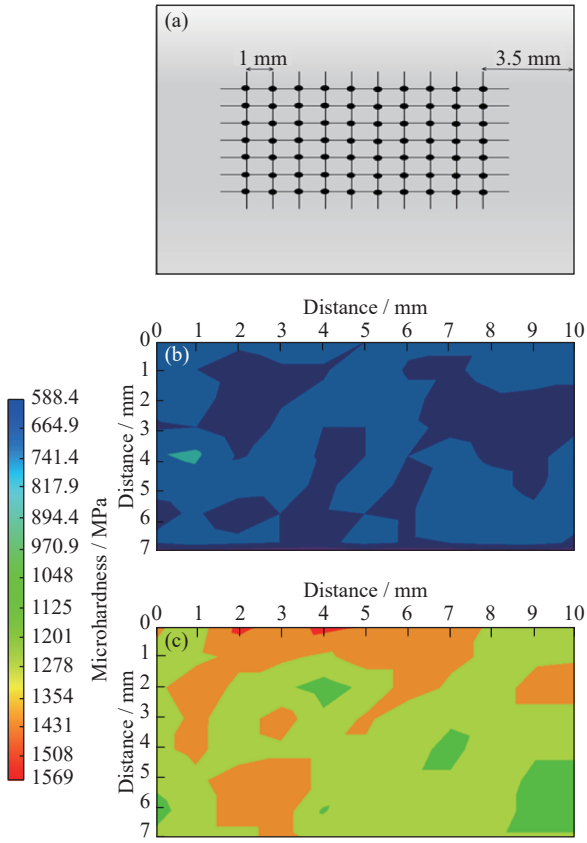

Fig. 6. (a) Distances between hardness measured points; hardness mappings for the (b) 0P and (c) 2P samples.

was also noticed. Comparing the obtained residual stress values for the 2P sample with the estimated YS (425 MPa), the maximum residual stress on the surface corresponded to 44% and 35% of the YS for the external and internal faces, respectively. Below 20 μm of the surface, these percentages dropped to 40% and 27%, which was attributed to the friction effect between the sample and the die walls. These are considerable amounts for those applications where the fatigue limit is important.

The peak broadening depicted in Fig. 8 is strongly related to the grain size and microdeformation generated by the ECAP process. The maximum broadening observed was between the 0P and 1P samples. As mentioned above, the typical contributions to the peak broadening are the microstrains or the second-order residual stress and the decrement of the crystalline domain. In this case, the grain size is larger than the instrumental limit (100 nm); therefore, the peak broadening will not be significantly affected by the grain size.

The Williamson-Hall method was employed to qualitatively measure the microstrains produced by ECAP (Fig. 9). Here, a change in the slope is related to the change in the strain; this can be explained in terms of the increase of dislocation density as a function of the applied deformation. This result is supported by the subgrain formation associated with the dislocation tangles, as previously shown in Fig. 4.

In general, the results showed a grain refinement that was concomitant with the texture evolution, with the ideal components for ECAPed FCC metals, and with the increment of macro- and micro-residual stresses following the applied deformation. The dislocation tangles observed by electron microscopy were related to the increase of hardness for the 2P sample; they were also caused by the intensification of microstrains as a function of the number of ECAP passes, which was also observed by XRD peak broadening. The effect of the friction process between the die and sample was evident from the surface down to 20 μm, observed by the residual stress profiles. The residual stresses showed compressive val-

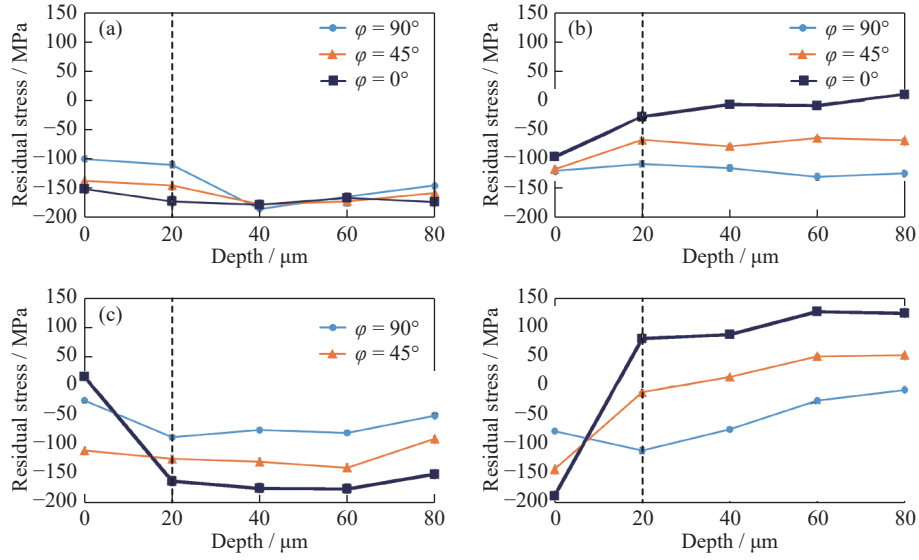

Fig. 7. Residual stress profiles for the 1P sample in the (a) external and (b) internal faces and the 2P sample in the (c) external and (d) internal faces. φ corresponds to the direction of the measurement.

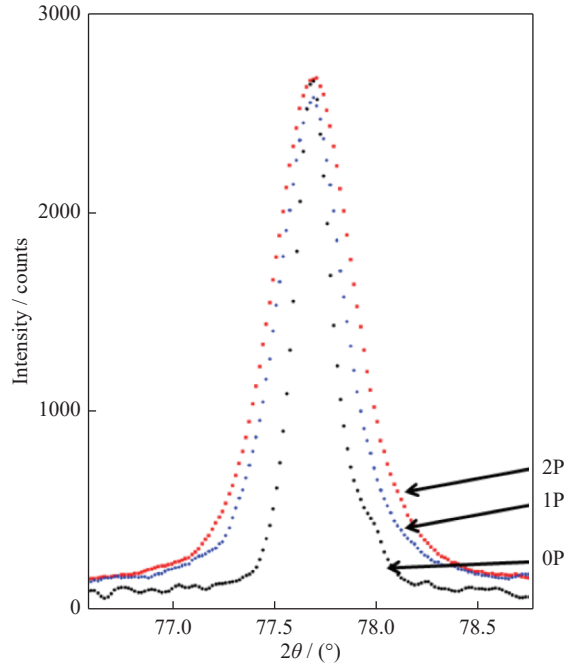

Fig. 8. Peak broadening as a function of deformation applied for the 0P, 1P, and 2P samples.

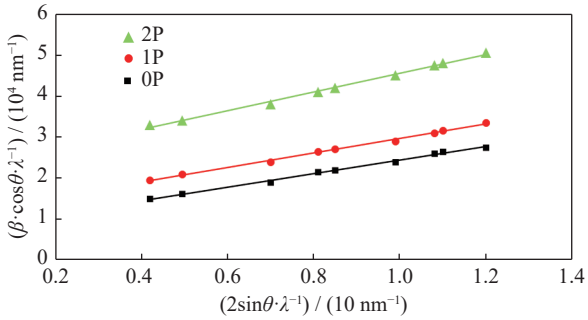

Fig. 9. Williamson-Hall plots for the 0P, 1P, and 2P samples, where β is the integral breadth, λ is the wavelength, and θ is the diffraction angle.

ues on the surface and down to 20 μm. This could be suitable for applications related to the stress corrosion cracking resistance [27–28].

4. Conclusions

The ECAP process via the Bc route was applied on a 5083 Al alloy until an equivalent deformation of ~1.26 was obtained. The microstructural characterization showed grain refinement after the first ECAP pass and the formation of subgrains after the second pass. The morphologies of the Mg_2Si and α-Al(Mn,Fe)Si precipitates for the 0P and 2P samples were similar. The hardness of the 2P sample was almost double of that obtained for the 0P sample. The 61.5% increment in hardness after the second extrusion pass and the XRD peak broadening indicated some degree of grain refinement. The loss of cube texture intensity was related to the formation of randomly organized new grains as a function of the ECAP passes, which was associated with subgrains formation. The observed texture components also corresponded with those of a simple shear process. Residual stresses of first and second orders showed an increase with the plastic deformation applied, having different stress states, depending on the measured face. The dislocation tangles observed by electron microscopy were related to the hardness increase of the 2P sample and caused by the intensification of microstrains, which was dependent on the number of ECAP passes. Finally, the heterogeneous hardness behavior was compatible with a highly localized dislocation density.

Acknowledgements

This project was financially supported by PAPIIT-UNAM through grants IN107917 and scholarship CONACyT (No. 592722). Valuable technical support provided by G. Lara, A. Tejeda, O. Novelo, J. Romero, C. Ramos, C. Flores, F. Garcia, and M. Jain is also acknowledged.

References

[1] T.L. Dickerson and J. Przydatek, Fatigue of friction stir welds in aluminum alloys that contain root flaws, *Int. J. Fatigue*, 25(2003), No. 12, p. 1399.

[2] T. Hirata, T. Oguri, H. Hagino, T. Tanaka, S.W. Chung, Y. Takigawa, and K. Higashi, Influence of friction stir welding parameters on grain size and formability in 5083 aluminum alloy, *Mater. Sci. Eng. A*, 456(2007), No. 1-2, p. 344.

[3] M.R. Toroghinejad, F. Ashrafizadeh, and R. Jamaati, On the use of accumulative roll bonding process to develop nanostructured aluminum alloy 5083, *Mater. Sci. Eng. A*, 561(2013), p. 145.

[4] G.E. Totten and D.S. MacKenzie, *Handbook of Aluminum: Vol. 1 Physical Metallurgy and Processes*, CRC press, Boca Raton, 2003.

[5] Z. Horita, T. Fujinami, M. Nemoto, and T.G. Langdon, Equal-channel angular pressing of commercial aluminum alloys: Grain refinement, thermal stability and tensile properties, *Metall. Mater. Trans. A*, 31(2000), p. 691.

[6] K.T. Park, S.H. Myung, D.H. Shin, and C.S. Lee, Size and distribution of particles and voids pre-existing in equal channel angular pressed 5083 Al alloy: Their effect on cavitation during low-temperature superplastic deformation, *Mater. Sci. Eng. A*, 371(2004), No. 1-2, p. 178.

[7] S.Y. Chang, B.D. Ahn, S.K. Hong, S. Kamado, Y. Kojima, and D.H. Shin, Tensile deformation characteristics of a nano-structured 5083 Al alloy, *J. Alloys Compd.*, 386(2005), No. 1-2, p. 197.

[8] J.C. Lee, S.H. Lee, S.W. Kim, D.Y. Hwang, D.H. Shin, and S.W. Lee, The thermal behavior of aluminum 5083 alloys deformed by equal channel angular pressing, *Thermochim. Acta*, 499(2010), No. 1-2, p. 100.

[9] P. Fernández, G. Bruno, and G. González-Doncel, Macro and micro-residual stress distribution in 6061 Al–15 vol.% SiC_w under different heat treatment conditions, *Compos. Sci. Technol.*, 66(2006), No. 11-12, p. 1738.

[10] S. Qu, X.H. An, H.J. Yang, C.X. Huang, G. Yang, Q.S. Zang,

Z.G. Wang, S.D. Wu, and Z.F. Zhang, Microstructural evolution and mechanical properties of Cu−Al alloys subjected to equal channel angular pressing, *Acta Mater.*, 57(2009), No. 5, p. 1586.

[11] Y.G. Kim, Y.G. Ko, D.H. Shin, and S. Lee, Effect of equal-channel angular pressing routes on high-strain-rate deformation behavior of ultra-fine-grained aluminum alloy, *Acta Mater.*, 58(2010), No. 7, p. 2545.

[12] Y. Iwahashi, J.T. Wang, Z. Horita, M. Nemoto, and T.G. Langdon, Principle of equal-channel angular pressing for the processing of ultra-fine grained materials, *Scripta Mater.*, 35(1996), No. 2, p. 143.

[13] G. Gonzalez, C. Braham, J.L. Lebrun, Y. Chastel, W. Seiler, and I.A. Figueroa, Microstructure and texture of Al2SixSn (x = 0, 4, 8 mass%) alloys processed by equal channel angular pressing, *Mater. Trans.*, 53(2012), No. 7, p. 1234.

[14] O. Engler, Z.S. Liu, and K. Kuhnke, Impact of homogenization on particles in the Al−Mg−Mn alloy AA 5454 − Experiment and simulation, *J. Alloys Compd.*, 560(2013), p. 111.

[15] J.E. Tibballs, J.A. Horst, and C.J. Simensen, Precipitation of α-Al(Fe,Mn)Si from the melt, *J. Mater. Sci.*, 36(2001), p. 937.

[16] J. Lacaze, L. Eleno, and B. Sundman, Thermodynamic assessment of the aluminum corner of the Al−Fe−Mn−Si system, *Metall. Mater. Trans. A*, 41(2010), p. 2208.

[17] O. Engler and S. Miller-Jupp, Control of second-phase particles in the Al−Mg−Mn alloy AA 5083, *J. Alloys Compd.*, 689(2016), p. 998.

[18] G.S. Yi, B.H. Sun, J.D. Poplawsky, Y.K. Zhu, and M.L. Free, Investigation of pre-existing particles in Al 5083 alloys, *J. Alloys Compd.*, 740(2018), p. 461.

[19] M. Kawasaki, Z. Horita, and T.G. Langdon, Microstructural evolution in high purity aluminum processed by ECAP, *Mater. Sci. Eng. A*, 524(2009), No. 1-2, p. 143.

[20] T.G. Langdon, The principles of grain refinement in equal-channel angular pressing, *Mater. Sci. Eng. A*, 462(2007), No. 1-2, p. 3.

[21] I.J. Beyerlein and L.S. Tóth, Texture evolution in equal-channel angular extrusion, *Prog. Mater. Sci.*, 54(2009), No. 4, p. 427.

[22] A.A. Tiamiyu, R. Basu, A.G. Odeshi, and J.A. Szpunar, Plastic deformation in relation to microstructure and texture evolution in AA 2017-T451 and AA 2624-T351 aluminum alloys under dynamic impact loading, *Mater. Sci. Eng. A*, 636(2015), p. 379.

[23] S.N. Alhajeri, N. Gao, and T.G. Langdon, Hardness homogeneity on longitudinal and transverse sections of an aluminum alloy processed by ECAP, *Mater. Sci. Eng. A*, 528(2011), No. 10-11, p. 3833.

[24] Y.T. Zhu, H.G. Jiang, J.Y. Haung, and T.C. Lowe, A new route to bulk nanostructured metals, *Metall. Mater. Trans. A*, 32(2001), No. 6, p. 1559.

[25] D. Tabor, *The Hardness of Metals*, Clarendon Press, Oxford, 1951.

[26] P.G. Sanders, J.A. Eastman, and J.R. Weertman, Elastic and tensile behavior of nanocrystalline copper and palladium, *Acta Mater.*, 45(1997), No. 10, p. 4019.

[27] D.P. Braga, D.C.C. Magalhães, A.M. Kliauga, C.A.D. Rovere, and V.L. Sordi, Microstructure, mechanical behavior and stress corrosion cracking susceptibility in ultrafine-grained Al−Cu alloy, *Mater. Sci. Eng. A*, 773(2020), art. No. 138865.

[28] J.T. Wang, Y.K. Zhang, J.F. Chen, J.Y. Zhou, M.Z. Ge, Y.L. Lu, and X.L. Li, Effects of laser shock peening on stress corrosion behavior of 7075 aluminum alloy laser welded joints, *Mater. Sci. Eng. A*, 647(2015), p. 7.